

RESEARCH ARTICLE

Development of a microchannel emulsification process for pancreatic beta cell encapsulation

Christina M.E. Bitar¹  | Karen E. Markwick¹  | Dušana Treľová²  |
Zuzana Kroneková²  | Michal Pelach² | Chloé M.O. Selerier¹  | James Dietrich³  |
Igor Lacík²  | Corinne A. Hoesli¹ 

¹Department of Chemical Engineering, McGill University, Montreal, Quebec, Canada

²Department for Biomaterials Research, Polymer Institute of the Slovak Academy of Sciences, Bratislava, Slovakia

³Advanced Radio Frequency Systems Laboratory, CMC Microsystems, University of Manitoba, Winnipeg, Manitoba, Canada

Correspondence

Corinne A. Hoesli, Canada Research Chair in Cellular Therapy Bioprocess Engineering, Department of Chemical Engineering, McGill University, Wong Building, 3610 University Street, Montreal, Quebec H3A 0C5, Canada. Email: corinne.hoesli@mcgill.ca

Present address

Karen E. Markwick, STEMCELL Technologies, 1618 Station St., Vancouver, British Columbia V6A 1B6, Canada

Funding information

Canada Research Chair (NSERC Tier 2), Grant/Award Number: 950-231290; Canadian Foundation for Innovation, project 35507; Centre québécois sur les matériaux fonctionnels; Fonds de Recherche du Québec - Nature et Technologies; NSERC Discovery Grant, Grant/Award Number: RGPIN-2015-06271; PROTEO, The Quebec Network for Research on Protein Function; Quebec Cell, Tissue and Gene Therapy Network-ThéCell (a thematic network supported by the Fonds de recherche du Québec-Santé); Slovak Research and Development Agency, Grant/Award Number: APVV-14-0858; Montreal Diabetes Research Center (MDRC)

Abstract

In this study, we developed a high-throughput microchannel emulsification process to encapsulate pancreatic beta cells in monodisperse alginate beads. The process builds on a stirred emulsification and internal gelation method previously adapted to pancreatic cell encapsulation. Alginate bead production was achieved by flowing a 0.5–2.5% alginate solution with cells and CaCO₃ across a 1-mm thick polytetrafluoroethylene plate with 700 × 200 μm rectangular straight-through channels. Alginate beads ranging from 1.5–3 mm in diameter were obtained at production rates exceeding 140 mL/hr per microchannel. Compared to the stirred emulsification process, the microchannel emulsification beads had a narrower size distribution and demonstrated enhanced compressive burst strength. Both microchannel and stirred emulsification beads exhibited homogeneous profiles of 0.7% alginate concentration using an initial alginate solution concentration of 1.5%. Encapsulated beta cell viability of 89 ± 2% based on live/dead staining was achieved by minimizing the bead residence time in the acidified organic phase fluid. Microchannel emulsification is a promising method for clinical-scale pancreatic beta cell encapsulation as well as other applications in the pharmaceutical, food, and cosmetic industries.

KEYWORDS

alginate, cellular therapy, emulsion, encapsulation, microchannel

1 | INTRODUCTION

Islet transplantation is now an established clinical intervention for the treatment of Type 1 diabetes in many jurisdictions, with 50–70% of

Christina M.E. Bitar and Karen E. Markwick contributed equally to this study.

This is an open access article under the terms of the Creative Commons Attribution-NonCommercial License, which permits use, distribution and reproduction in any medium, provided the original work is properly cited and is not used for commercial purposes.

© 2019 The Authors. *Biotechnology Progress* published by Wiley Periodicals, Inc. on behalf of American Institute of Chemical Engineers.

patients remaining insulin independent for ~5 years post transplantation.¹ Islet encapsulation has the potential to eliminate the requirement of life-long immune suppression,²⁻⁴ while broadening the cell supply to include pluripotent stem cells and xenogeneic islet sources.^{5,6}

Traditional nozzle-based encapsulation devices have an alginate viscosity operating range between 0.03 Pa·s and 11 Pa·s and throughputs typically <2 L/hr.⁷⁻¹⁰ Since the resulting alginate beads are generally permeable to antibodies, a variety of cationic polymer coatings have been applied to reduce the pore size and increase bead stability. However, this has been correlated with increased fibrotic overgrowth of the beads.^{11,12} Another method to reduce bead porosity is to encapsulate cells in high-concentration alginate beads that can be obtained by stirred emulsification and internal gelation.^{13,14} This cell encapsulation process, adapted from a method originally described by Poncelet et al.,¹⁵ can be scaled to m³/hr production rates of alginate beads using solutions with viscosities exceeding 100 Pa·s.¹⁴ Since the local energy dissipation rate varies greatly in turbulent flow as applied in the stirred emulsification process, a broad bead size distribution is obtained. Polydisperse beads may influence the islet survival given the risks of incomplete islet encapsulation in smaller beads¹⁶ and oxygen limitations in larger beads.¹⁷ More recently, islets encapsulated in larger (1.5 mm) alginate beads transplanted into allogeneic primate animal models survived and remained functional for at least 4 months.¹⁸

A device that can accommodate a broad alginate viscosity operating range and produce uniform beads at clinical-scale throughputs is desirable. Microchannel emulsification was previously used to produce monodisperse oil-in-water emulsion droplets of 1 μm to several millimeters in diameter.¹⁹⁻²¹ The droplets form spontaneously due to the hydrodynamic instability of the dispersed phase exiting the channels, unlike in membrane emulsification where external shear stresses facilitate droplet formation.²² Up to a critical transition point, identified by the critical capillary number, the droplet diameter is independent of the inlet dispersed phase flow rate, rendering the microchannel emulsification process highly robust and scalable.

The encapsulation of human embryonic kidney cells in 50–200 μm alginate beads was achieved at 20 mL/hr production rates using 100 microchannel arrays.²³ The external gelation method applied in this process relied on the contact and coalescence between alginate droplets and CaCl₂ solution droplets in the flowing oil phase, resulting in a significant proportion of deformed beads.²³ Moreover, in the context of islet encapsulation, larger beads would be desirable to encapsulate ~150 μm diameter (or larger) cell clusters.

Here, we describe a novel microchannel emulsification and internal gelation process to encapsulate pancreatic beta cells in monodisperse alginate beads. Process development involved the design and characterization of the novel system that can produce uniform (<10% variation) 1.5–3 mm alginate beads for animal cell encapsulation at throughputs required for clinical islet transplantation (>100 mL/hr).¹⁴ These results were achieved by investigating the effects of various process parameters (e.g., density, surface tension, viscosity, and flow rate) on bead size and uniformity. Successful encapsulation of insulin-

producing beta cells was achieved by optimizing the acetic acid concentration as well as the bead residence time in acid.

2 | MATERIALS AND METHODS

2.1 | Dispersed phase preparation

Unless otherwise mentioned, all reagents were purchased from Thermo Fisher Scientific. Alginate (FMC Manugel® GHB alginate, FMC Bio-Polymer, Lot # G0600201) was dissolved in HEPES 4-[2-hydroxyethyl]-1-piperazineethanesulfonic acid (HEPES)-buffered saline solution (10 mM HEPES, 170 mM NaCl from Sigma-Aldrich, pH 7.4) and then autoclaved for 30 min. Autoclaving reduced the weight average molecular weight from 135 to 75 kDa as determined by a size-exclusion chromatography system equipped with multiangle light scattering detector.²⁴ Complete cell culture medium consisted of Dulbecco's modified Eagle medium supplemented with 10% fetal bovine serum (FBS), 1% penicillin/streptomycin, 2 mM L-glutamine, and 5 mM β-mercaptoethanol (Sigma-Aldrich). The CaCO₃ suspension consisted of 0.05 g/mL CaCO₃ in HEPES-buffered saline solution. The to-be-dispersed phase was prepared by mixing alginate solution (29.7 mL), complete medium with or without cells (2.3 mL), CaCO₃ suspension (1.65 mL), and FBS (1 mL).

2.2 | Surface tension and viscosity measurements

Fluid surface tension was measured using a DCAT 9 Dynamic Contact Angle Meter and Tensiometer (Particle and Surface Sciences Dataphysics) at motor speeds of 1 and 0.1 mm/s for continuous phase fluids and alginate solutions, respectively. Dynamic viscosity measurements of alginate solutions at 25 and 37°C over a shear rate range of 0–600/s were performed using an Anton Paar MCR 302 rheometer with a double gap configuration. The effect of shear rate on alginate viscosity was fitted to the Cross model,²⁵ while the effect of alginate concentration on zero-shear viscosity was described by the Huggins equation.²⁶

2.3 | Microchannel plate fabrication

Three-dimensional (3D)-printed plastic plates were printed by Shapeways (New York, NY) using ultraviolet (UV)-cured Frosted Ultra Detailed Plastic. Laser micromilling (355 nm UV diode-pumped solid-state picosecond-pulsed laser system from Oxford Lasers, Inc.) was used to create microchannels through 1-mm thick polytetrafluoroethylene (PTFE) and fluorinated ethylene propylene (FEP) sheets (McMaster-Carr). Channels were tapered with average dimensions of 700 × 200 μm. The laser mill parameters were 35 mW power, 400 Hz repetition rate, 0.1 mm/s feed rate, 40 μm spot size, and 15 μm hatch pitch. Under these conditions, channels with clean edges were achieved after 10 passes, stepping the focusing lens 200 μm closer after 5 passes.

2.4 | Contact angle measurements

Contact angles between a static droplet (<30 μL) of various solvents (water, 1-octanol, and toluene) and the microchannel plates were

determined using an OCA 150 system goniometer (DataPhysics Instruments GmbH) and SCA-20 software. The solid–liquid interfacial free energy (γ_{SL}) was obtained by Young's equation and the Owens–Wendt method.²⁷

2.5 | Microencapsulation by microchannel emulsification

A novel microchannel emulsification device prototype was fabricated as illustrated in Figure 1. The device consisted of two flow chambers flanking a microchannel plate comprising one to three straight-through microchannels ($700 \times 200 \mu\text{m}$). Above the top chamber was an outlet tube (1.3 cm in diameter) leading to a collection vessel ($8.0 \times 12.0 \times 8.8 \text{ cm}$). The bottom chamber with alginate phase was connected to a Sage Instruments model 355/365 syringe pump (Cole-Parmer). Although an inlet port was included in the device prototype design to allow fluid flow in the top chamber, no flow was applied in reported experiments. For cell encapsulation studies, MIN6 cells were suspended in the complete medium at 13×10^6 cells/mL prior to preparing the dispersed phase fluid as described above. The dispersed phase fluid was transferred into a 30-mL syringe (VWR International) mounted onto the syringe pump and the syringe was then pushed manually to fill the bottom chamber. The continuous phases tested were 3M™ Novec™ 7500 (3M Company), light mineral oil (O121-4, Thermo Fisher Scientific), or glyceryl trioleate (~65%, Sigma-Aldrich). The continuous phase fluids were acidified by adding 0.22% glacial acetic acid and vortexed prior to use. Next, 200 mL of the acidified continuous phase was poured into the collection vessel to fill the top chamber. Alginate flow was initiated at 10 mL/min to purge air from the channels and then reduced to the flow rate to be tested (0.55 mL/min unless otherwise specified) to initiate droplet

generation. The beads were left in the collection vessel for a gelation time of up to 10 min before separation using a $40 \mu\text{m}$ nylon cell strainer and washing ($3 \times$ in complete medium). The gelation time represents the time after the first droplet is generated.

2.6 | Full factorial design of experiments

The effects of the final alginate concentration in the dispersed phase (C_i with low level 0.5% and high level 2.5%) and the inlet alginate phase flow rate (F_i with low level 0.31 mL/min and high level 0.78 mL/min) on the average bead diameter (Y) were assessed via a 2^2 full factorial design of experiment with three center points and two replicates. Results were fitted to a linear model:

$$Y = \beta_0 + \beta_1 X_1 + \beta_2 X_2 + \beta_3 X_1 X_2, \quad (1)$$

where $X_1 = (C_i - 1.5\%)/1\%$, $X_2 = (F_i - 0.55 \text{ mL/min})/0.24 \text{ mL/min}$, $X_1 X_2$ is the interaction between alginate concentration and flow rate, and β_i values represent regression coefficients.

2.7 | Alginate bead size distribution

As previously described,¹³ 1 mL of alginate beads were incubated in 5 mL of 0.02 g/L Toluidine Blue O (Sigma-Aldrich) in HEPES-buffered saline solution for 80 min on a rotary shaker. A photo of the stained beads dispersed in HEPES-buffered saline solution (with 10% complete medium) was taken using an iPhone 6s 12-megapixel camera (Apple). CellProfiler freeware²⁸ was used to determine the mean diameter, Sauter mean diameter (D_{32}), and volume moment mean diameter (D_{43}).^{13,14}

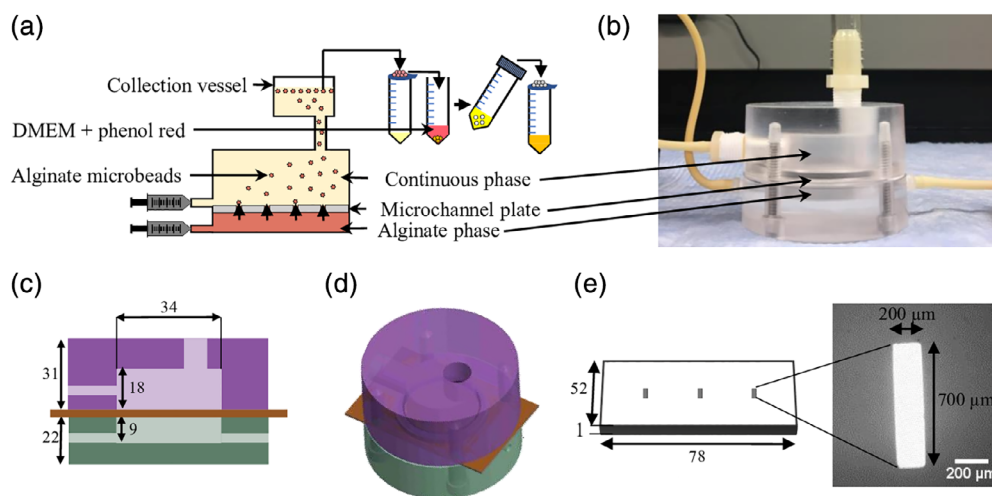


FIGURE 1 Schematic illustration of the microchannel emulsification process and apparatus. (a) Beads were produced via microchannel emulsification and internal gelation followed by rinsing in complete medium (three times or until phenol red indicator no longer changes in color) prior to further product assessment. (b) Photo of the microchannel emulsification device consisting of a top (oil phase) and bottom (alginate phase) chamber as well as a polytetrafluoroethylene (PTFE) plate in between with three oblong ($700 \times 200 \mu\text{m}$) microchannels in parallel. (c) Two-dimensional drawing of the front view of the device with dimensions in mm. (d) Three-dimensional (3D) computer-assisted design drawing of the device. (e) 3D drawing of the PTFE plate along with a microscope image of a laser micromilled channel on the plate

2.8 | Bead production by stirred emulsification

Alginate beads of D_{32} matching the microchannel emulsification process bead diameters (~ 2 mm) were produced using a stirred emulsification and internal gelation process as previously described,^{13,29} except that the initial continuous phase (light mineral oil) volume was 20 mL instead of 10 mL. Briefly, 20 mL of light mineral oil was introduced into a 100-mL microcarrier spinner flask of previously described dimensions^{13,29} placed on a calibrated magnetic stir plate to apply 190 rpm rotational speed to the impeller. Next, 10.5 mL of the to-be-dispersed phase was slowly introduced into the vessel and emulsified for 12 min before adding 10 mL of acidified mineral oil (0.4% acetic acid, leading to a final concentration of 0.13% in the total 30 mL mineral oil). After 8 min of internal gelation, agitation was stopped, and beads were collected in complete cell culture medium.

2.9 | Mechanical properties, permeability to immunoglobulin G, and spatial distribution of alginate

Beads produced by microchannel or stirred emulsification were transferred to filtered (Stericup® and Steritop®, 0.22 μ m, Millipore) storage solution (2 mM CaCl₂ and 100 ppm NaN₃ in HEPES-buffered saline solution) at a 1:10 volumetric ratio and shipped to the Polymer Institute of the Slovak Academy of Sciences (SAS) for characterization of their physicochemical properties. The bead mechanical strength expressed as the bursting force was determined from the compression deformation at a compression speed of 0.5 mm/s using a Texture Analyzer (Stable Micro Systems, Godalming, United Kingdom). To match the size of both types of beads for this analysis, the measurements were done on hand-picked beads in the size range of 2–2.5 mm.

The permeability of beads to immunoglobulin G (IgG) was evaluated by confocal laser scanning microscopy (CLSM) using Alexa Fluor 488-labelled IgG antibodies (Life Technologies, Molecular Probes).³⁰ Approximately 10 beads were placed in a 1.5-mL Eppendorf tube and the storage solution was replaced by a storage solution containing 0.02 mg/mL IgG-Alexa Fluor 488. The tube was incubated at 37°C on a rocking platform (2 rpm) for 24 hr. The images of six different beads with the focus on their equatorial plane were acquired using LSM510 META on Axiovert 200 (both Zeiss) and 10 \times Apochromat objective. For each bead, the mean intensity from its inner region (I_{in}) and the mean intensity of the staining solution outside the bead (I_{out}) were measured. The permeation of IgG into beads was expressed as P (%) = $I_{in}/I_{out} \times 100$, where the intensities represent the mean intensities acquired from six beads.

Spatial distribution of alginate in the beads was determined using a confocal Raman microscope (CRM) WITec alpha300R (WITec, Ulm, Germany) equipped with a water immersion objective (Carl Zeiss 20 \times /1NA), and the WITec UHTS300 spectrometers, at a controlled room temperature of 23°C. The 785-nm laser line was used for excitation of Raman signal with an integration time of 10 s. Data acquisition and evaluation, including the quantitative analysis of alginate concentration, were performed as previously described.³¹

2.10 | MIN6 cell culture and viability staining

MIN6 cells³² were obtained from Dr James Johnson (University of British Columbia) and cultured at 4×10^4 cells/cm² seeding density on surface-treated T-flasks (Sarstedt), in 0.27 mL/cm² complete medium that was replenished every 2 days. The cells were passaged using TrypLE at $\sim 90\%$ confluency. Cells were enumerated using a hemocytometer (Hausser Scientific) after staining with 0.2% Trypan blue solution (Sigma-Aldrich). Dead encapsulated cell controls were incubated in 5 mL of 99% ethanol for 10 min prior to live/dead staining or flow cytometry. Immobilized cells were stained for 30 min in live/dead staining solution (4 μ M calcein AM, 4 μ M ethidium homodimer, 8 μ M Hoechst in HEPES-buffered saline solution) prior to fluorescence microscopy (IX81, model IX2, Olympus, Tokyo, Japan). For flow cytometry, immobilized cells were added to a degelling solution (55 mM sodium citrate dihydrate from Sigma-Aldrich, 10 mM HEPES, and 95 mM NaCl, pH 7.4) at a 1:9 volumetric ratio and incubated on a rotary shaker on ice at 90 rpm for 40–60 min. The cells were then resuspended in propidium iodide solution (12.5 μ g/mL in phosphate-buffered saline solution, BD Life Sciences), incubated at 4°C for 30 min, and analyzed by a BD Accuri C6 flow cytometer. FlowJo Single Cell Analysis v10 was used for data analysis.

2.11 | Statistics

Differences between groups ($p < .05$ unless otherwise stated) were identified by two-tailed t tests or one-way analysis of variance (for multiple test conditions) followed by Tukey and Scheffe post hoc tests using JMP software (SAS Institute). Unless otherwise mentioned, results shown represent the average \pm standard error of the mean (SEM) of three independent experiments.

3 | RESULTS AND DISCUSSION

3.1 | Continuous phase fluid selection

Selection of a continuous phase fluid that would promote droplet formation in the microchannel emulsification device was conducted to determine the orientation of the device, which depends on whether the oil or aqueous phase is heavier. To promote droplet generation, factors that drive droplet detachment (e.g., the density difference between the phases) were maximized while forces counter-acting droplet generation (e.g., interfacial tension) were minimized. We compared the density difference and surface tension of various organic phase fluids (3M™ Novec™ Engineered Fluid, light mineral oil, and glyceryl trioleate) under the assumption that lower surface tensions correlate with lower interfacial tensions. The alginate concentration in the range of 0.5–1.5% did not significantly affect the surface tension value of 0.055 ± 0.001 N/m. Novec™ 7500 fluid (density 1,630 kg/m³) had the highest density difference with a 1.5% alginate solution (density 1,020 kg/m³) and the lowest surface tension (Figure 2), both of which favored the formation of smaller alginate droplets. The selection of the heavier Novec™ 7500 led to a

microchannel emulsification prototype design with the alginate flowing below the microchannel plate and the oil phase above.

3.2 | Device design and plate material selection

A dual flow chamber device was designed (Figure 1) based on the following criteria: (a) sufficient microchannel plate surface to allow the eventual use of 25×25 microchannel arrays with ~ 2 mm distance between channel centers; (b) sufficient bead travel distance between the microchannel and the top wall to allow bead detachment without contacting the wall; (c) inlet ports for alginate and oil as well as an outlet for bead collection; (d) sufficient vertical distance between the collection vessel and the main device chamber to limit bead coalescence prior to transfer to the collection vessel. To promote droplet detachment in water-in-oil microchannel emulsification, a hydrophobic plate material was required such that the continuous phase would preferentially wet the microchannel surface.³³ All three materials considered (PTFE, FEP, and 3D-printed plastic) were hydrophobic with water contact angles $>90^\circ$. Table 1 presents the component and total surface free energies of PTFE, FEP, and 3D-printed plastic. The contact angle of toluene on a 3D-printed plastic surface was reported to be 0° , as complete wetting was observed. The experimentally determined surface free energies of PTFE and FEP were of the same order of

magnitude as values reported in the literature: 20.0 mJ/m^{34} and $17.9 \text{ mJ/m}^{2,35}$ respectively. As expected, the surface free energy of PTFE was higher than FEP, suggesting that PTFE would enhance wetting of the continuous phase fluid in the microchannel emulsification process.³⁶ For this reason, we continued using PTFE as the microchannel plate material for further microchannel emulsification experiments.

Oblong straight-through microchannels of aspect ratio exceeding 3.5 were previously shown to minimize the droplet diameter/microchannel diameter ratio by maximizing the instability of droplets exiting the channel, with a ratio of 2:1 achievable with suitable emulsifiers.^{37,38} The target channel dimensions were determined to be $700 \times 200 \mu\text{m}$ to theoretically achieve a target diameter of $\sim 600 \mu\text{m}$.³⁹ The first microchannels were produced in a plate with a thickness of $500 \mu\text{m}$. However, these channels resulted in continuous outflow and jetting of the to-be-dispersed phase. Given that the dispersed phase is destabilized along the length of the channel, it was hypothesized that increasing the length of the channel would improve formation and pinch-off of the dispersed phase neck. A plate thickness of 1 mm resulted in robust pinch-off and bead production. 3D-printed channels could only be printed in an oval shape with minimum achievable dimensions of $\sim 640 \times 240 \mu\text{m}$. Using the highest resolution material, Frosted Extreme Detail Plastic (Shapeways, USA), the material caved in and occluded the channels. Figure 1e displays smooth rectangular microchannels obtained by laser micromilling a 1-mm thick PTFE plate achieving both an aspect ratio of 3.5 and dimensions of $700 \times 200 \mu\text{m}$. In contrast, laser-micromilled FEP resulted in rough channel edges, leading to between-channel variability. Considering the solid surface energy and dimensional fidelity of the microchannels, the most promising microchannel fabrication technique was laser micromilling of PTFE.

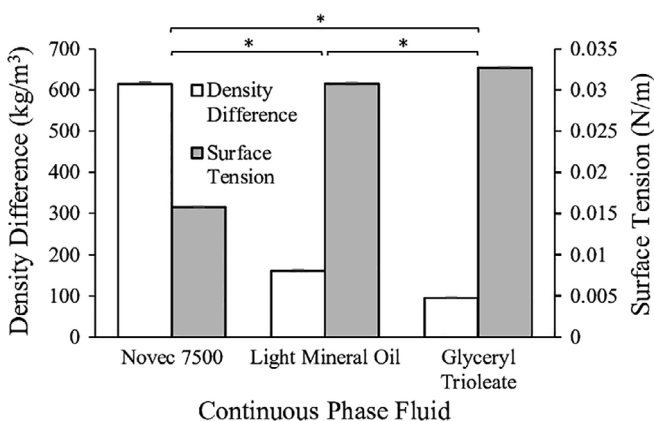


FIGURE 2 Surface tension of various continuous oil fluids (3M™ Novec™ Engineered Fluid, light mineral oil, and glyceryl trioleate) and density difference between these oil phases and a 1.5% alginate phase. * $p < .05$ for both density difference and surface tension

3.3 | Effect of alginate viscosity and flow rate on bead diameter

The main factors that drive droplet detachment in microchannel emulsification, and therefore dictate bead diameter, are interfacial tension and buoyancy forces up to a certain dispersed phase flow rate. This limit is dictated by the critical capillary number, above which prolonged droplet formation or continuous outflow of the alginate fluid

TABLE 1 Contact angles of solvents on various microchannel materials and the component (γ_s^d and γ_s^p) and total (γ_s) solid surface free energies

Solid surface material	Solvent	Average contact angle ($^\circ$)	γ_s^d (mJ/m ²)	γ_s^p (mJ/m ²)	γ_s (mJ/m ²)
PTFE	Water	106 ± 2	28 ± 1	0.1 ± 0.1	28 ± 1
	Toluene	23 ± 2			
FEP	Water	103 ± 1	21 ± 1	0.8 ± 0.2	22 ± 1
	Toluene	40 ± 1			
3D-printed plastic	Water	121 ± 5	36 ± 13	2 ± 14	38 ± 30
	Toluene	0			

Abbreviations: PTFE, polytetrafluoroethylene; FEP, fluorinated ethylene propylene.

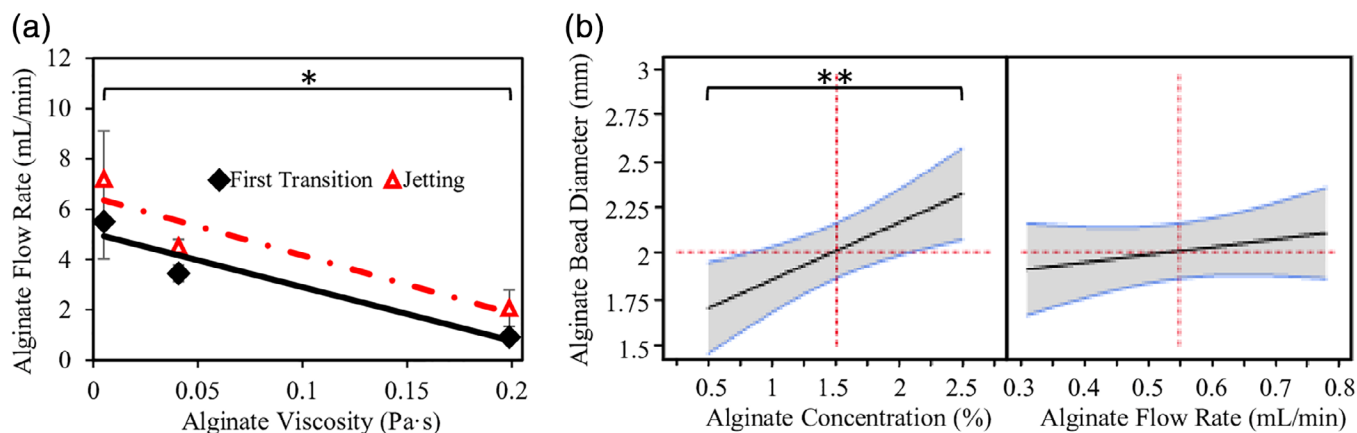


FIGURE 3 Characterization of the alginate flow regime through microchannels and the average bead diameter as a function of viscosity and flow rate. (a) Alginate flow rate resulting in first transition (droplet elongation with a neck) and jetting at a system temperature 25°C as a function of alginate viscosity. (b) Effect of alginate viscosity and flow rate on average bead diameter. This response plot was obtained directly from the Prediction Profiler plot generated by JMP statistical software. The blue curves represent the confidence intervals, and the intersection of the dotted red lines on each plot represents the point at which the data in the other plot is presented. * $p < .05$ (first transition only); ** $p < .01$

TABLE 2 Alginate fluid properties used in the calculation of the critical capillary numbers for each alginate concentration in this flow system at $T = 25^\circ\text{C}$

Alginate concentration (%)	Alginate viscosity (Pa·s)	Calculated average fluid velocity in the channel (m/s)	Critical capillary number ^{a,b}
0.5	0.01	0.66 ± 0.18	0.08 ± 0.02
1.5	0.04	0.41 ± 0.04	0.39 ± 0.04
2.5	0.20	0.11 ± 0.02	0.51 ± 0.08

^aThe dispersed phase critical capillary number (Ca_d) was calculated by $Ca_d = \eta_d U / \gamma$, where η_d is the dispersed phase viscosity, U is the velocity of the dispersed phase through the microchannel when first transition was observed, and γ is the equilibrium interfacial tension between the dispersed and continuous phases.⁴¹

^bThe interfacial tension value used for the critical capillary number calculation was obtained from the literature for a similar Novec/water system: 43 mN/m.⁴²

occurs.³³ The critical capillary number is useful in identifying the flow transition from droplet formation to elongated droplet formation with a neck (first transition) followed by continuous outflow of the dispersed phase (jetting).⁴⁰ As shown in Figure 3a, increasing the alginate viscosity decreased the alginate flow rate (and hence the velocity) required to reach first transition and jetting, as expected based on the capillary number relation. To identify the dispersed phase flow rate operating range within which uniform droplets are formed, critical capillary numbers for alginate solutions of different concentrations (Ca_d), summarized in Table 2, were estimated by $Ca_d = (\eta_d U / \gamma)$, where η_d is the dispersed phase viscosity, U is the velocity of the dispersed phase through the microchannel when first transition was observed, and γ is the equilibrium interfacial tension between the dispersed and continuous phases.⁴¹ The critical capillary number increased with alginate viscosity even though the flow rate resulting in jetting had a decreasing trend. This trend suggests that interfacial phenomena

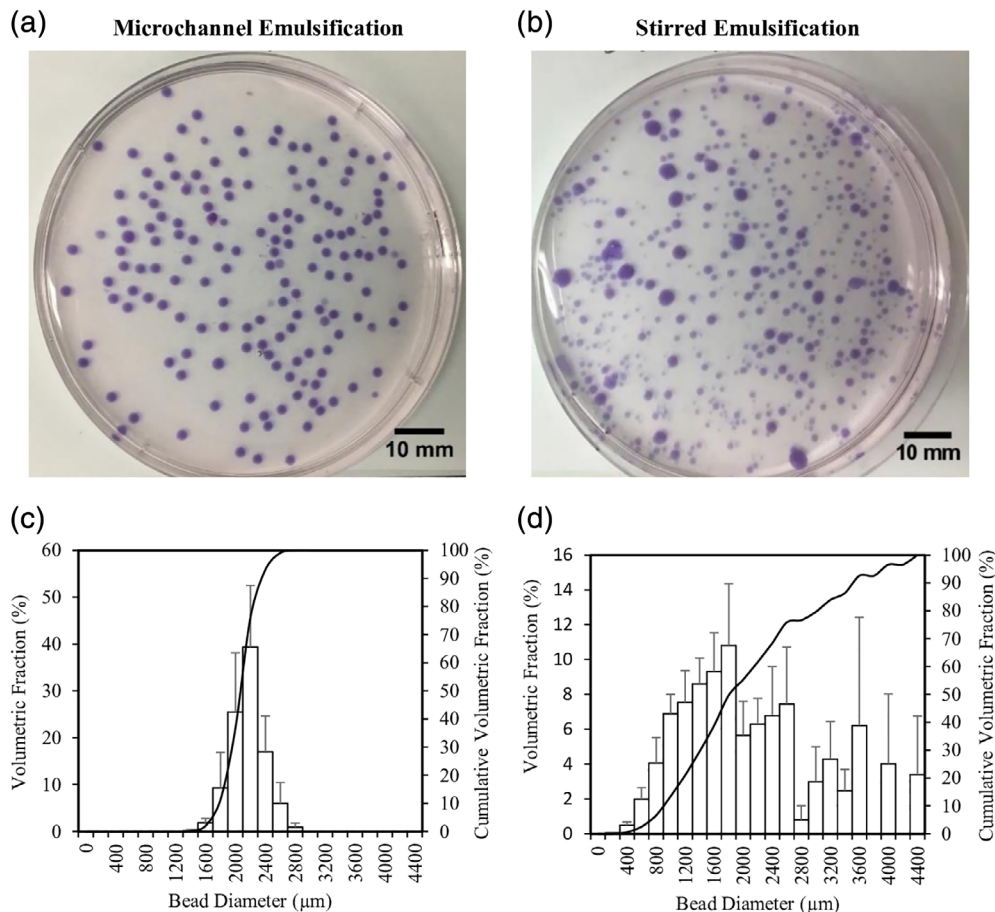
alone are insufficient to predict the mechanisms at play in the transition between jetting and droplet formation in this situation. The calculated critical capillary number at an alginate concentration of 1.5% (0.39 ± 0.04) was similar to literature values of 0.3.⁴³

A 2² full factorial design of experiments was then conducted to assess the significance of the effects of alginate viscosity, alginate flow rate, and the interaction of the two, on the average alginate bead diameter. Increasing the alginate concentration from 0.5% to 2.5% (i.e., viscosity increases from 0.01 Pa·s to 0.20 Pa·s) resulted in a significant increase in the average bead diameter (Figure 3b). As the alginate concentration did not affect the fluid surface tension, viscous forces appear to impact droplet formation at these concentrations. In contrast, the effect of the alginate flow rate on the average bead diameter was not found to be statistically significant over the range of 0.31–0.78 mL/min. The interaction between concentration and flow rate was also not found to be statistically significant. These results imply that the bead production rate can be altered without an undesirable change in bead diameter; however, tuning the alginate viscosity would alter the bead size. These observations are consistent with previous reports showing that increasing the dispersed phase average velocity in each channel increases droplet production frequency with limited impact on droplet diameter up to a critical point, which depends on the viscosity ratio between the phases.⁴⁴

3.4 | Bead size distribution

To determine whether the microchannel emulsification system leads to the expected increase in bead uniformity compared to the existing stirred emulsification process, the bead size distributions were measured for both processes (Figure 4). The average D_{32} of 1.5% alginate obtained by microchannel emulsification was $2,141 \pm 81 \mu\text{m}$ (SEM) with an average coefficient of variation of $9.1 \pm 0.5\%$. The rotational speed during stirred emulsification was successfully adjusted to achieve a similar D_{32} . As expected, the beads produced using the

FIGURE 4 Size distribution determined for beads produced from 1.5% alginate solution by (a) microchannel, (b) stirred emulsification, as well as (c,d) the respective bead size distributions. The coefficients of variation of the microchannel and stirred emulsification beads were 9% and 65%, respectively



microchannel emulsification were much more uniform in size compared to the beads produced using stirred emulsification (coefficient of variation of $65 \pm 6\%$). The sporadic production of smaller diameter beads in the microchannel emulsification process was noted both during the process and in the resulting beads, potentially due to the temporary obstruction of a microchannel. The average microchannel emulsification bead diameter to microchannel diameter ratio was significantly higher than 2, suggesting that smaller beads could be obtained with appropriate emulsifier selection. We previously used bovine serum albumin as an emulsifier when transplanting stirred emulsification beads,¹⁴ but other cytocompatible transplantation-grade emulsifiers could be considered.

3.5 | Bead physicochemical properties

This work resulted in alginate beads prepared by a novel method of microchannel emulsification. It is desirable to establish that this mode of bead formation leads to bead characteristics suitable for an intended application. Specifically, microspheres developed for cell therapies must fulfill strict criteria.⁴⁵ In this work, we compared selected physicochemical characteristics of newly prepared beads by microchannel emulsification with the characteristics of beads produced using the stirred emulsification method.^{13,14}

CRM imaging, recently introduced as a powerful tool for visualization of spatial distribution of polymers in hydrogel microspheres,³¹

was employed to determine the local concentration of alginate within the bead profile. Generally, the spatial distribution of polymers impacts the principal properties of microspheres such as chemical and mechanical stability, molecular weight cut-off, diffusion properties, and cell microenvironment.³¹ Figure 5 shows the representative alginate concentration profiles for beads produced by microchannel emulsification (Figure 5a) and stirred emulsification (Figure 5b) processes. These profiles are comparable showing a homogeneous spatial distribution of alginate throughout the bead with an alginate concentration of around 0.7%. The combined plot using a normalized distance and the averaged data from imaging of several beads of each type confirms practically identical alginate concentration for both types of beads (Figure 5c). This is expected behavior, since both processes used the same alginate, CaCO_3 concentration, and duration of acidification. A higher concentration of acid in the microchannel emulsification than in the stirred emulsification process was used (0.22% vs. 0.13% acetic acid) that did not seem to influence the absolute alginate concentration, consistent with a calcium or guluronic acid residue-limited reaction. This concentration of 0.7% in the beads is about twofold lower than the nominal concentration in the alginate solution. This indicates that both types of beads are susceptible to swelling likely resulting from bead washing and storage conditions after preparation. Based on the alginate concentrations in solution and in the beads, one can calculate that the size of the alginate droplet formed is 1.6 mm for a bead size of 2.0 mm. This relatively weak

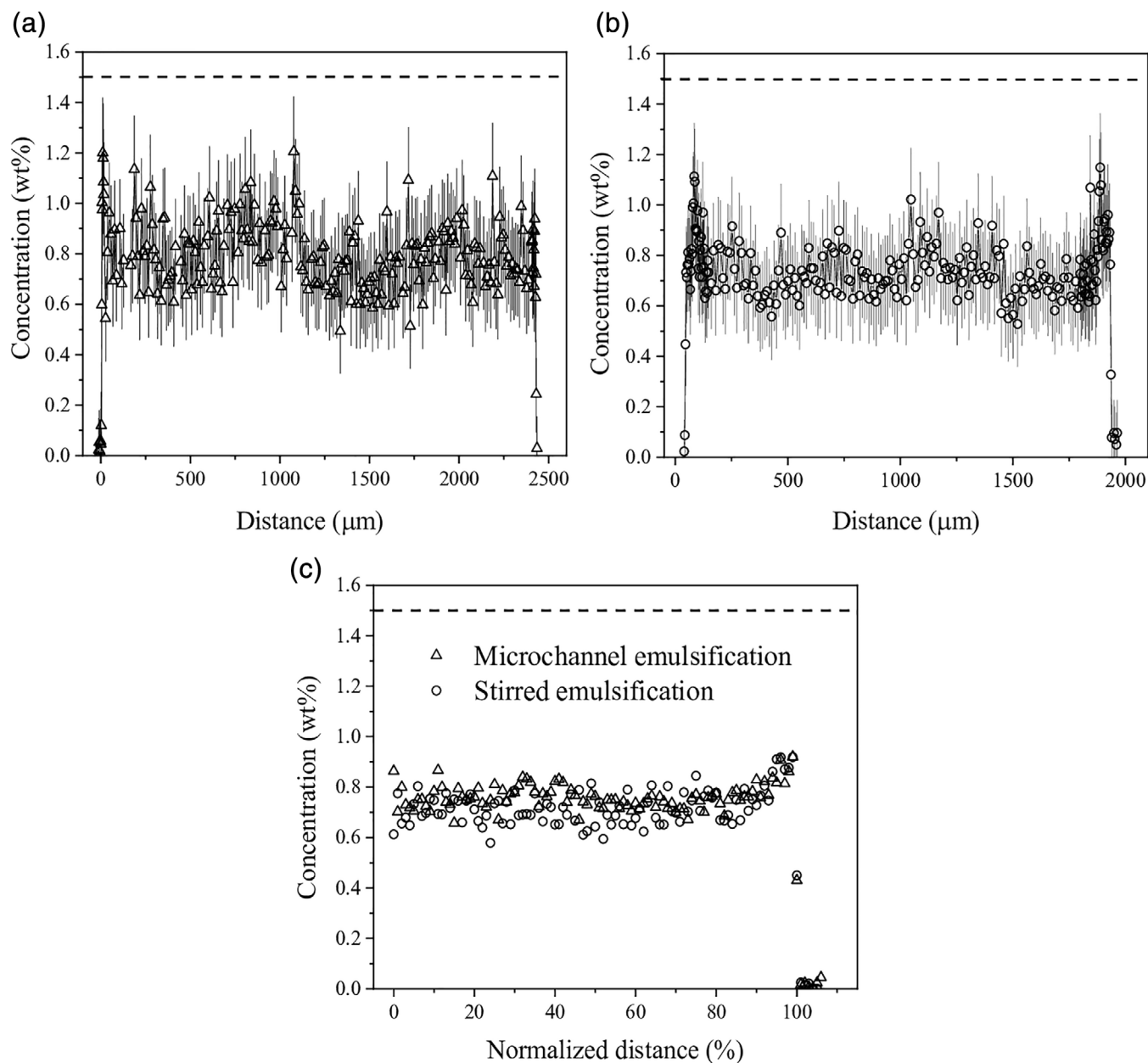


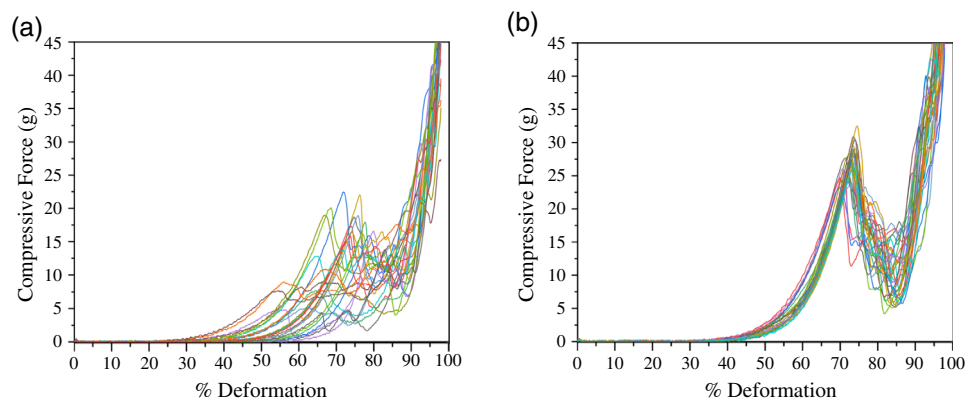
FIGURE 5 Concentration profiles for alginate beads determined by confocal Raman microscopy imaging for (a) microchannel emulsification beads and (b) stirred emulsification beads. (c) Combined alginate concentration profiles made of averaged profiles for five microchannel emulsification beads and four stirred emulsification beads. In order to directly compare beads of different sizes, the profiles are plotted against the normalized distance that is calculated as $M/R \times 100$, where R is radius and M is distance within R , providing 0% in the centre and 100% at the bead surface, respectively. Dashed lines represent the initial concentration of alginate in solution equal to 1.5%

crosslinking density of formed alginate beads is also reflected in the high IgG permeability values of 83% for both bead types. On the other hand, these data are not surprising as alginate beads of similar nominal alginate concentration made by a more typical external gelation process were found to be permeable to IgG.^{30,46}

Interestingly, the microchannel emulsification beads exhibited a higher mechanical stability compared to the stirred emulsification beads that can be related to a higher acid concentration in the microchannel emulsification process. The bursting force values determined from the uniaxial compression deformation tests were 27.3 ± 0.4 g

and 14 ± 1 g, respectively. The compression curves shown in Figure 6 also indicate that the microchannel emulsification beads were more homogeneous throughout the batch compared to the stirred emulsification beads (much like the bead size uniformities). The bursting force of the stirred emulsification beads was higher than the previously reported strength for smaller 1.5% alginate beads (average diameter of ~ 700 μm) produced via the same stirred emulsification process (~ 0.5 g).¹⁴ This means that once smaller beads are produced using microchannel emulsification, the bursting force of the beads will likely decrease. However, the bursting force for alginate-based microcapsules

FIGURE 6 Characterization of bead mechanical properties expressed as the bursting force for (a) microchannel emulsification beads and (b) stirred emulsification beads



being transplanted in the peritoneal cavity and subcutaneous space of rats was reported to be as low as 0.91 g^{47} ; there is thus ample room for a reduced compressive burst strength as a result of smaller beads.

3.6 | MIN6 cell survival

As a first step toward assessing the suitability of the microchannel emulsification process for animal cell encapsulation, MIN6 beta cell viability was measured before and after microchannel emulsification. In the stirred emulsification process, acidification rather than emulsification led to the greatest drop in cell viability.¹³ The acetic acid concentration in the microchannel emulsification process (0.22%) was higher than that in the stirred emulsification process (0.13%), which may potentially lead to a higher pH drop and increased cell death. To minimize cell losses in the microchannel emulsification process, the time the alginate beads reside in the acidified continuous phase (acidification time) should be minimized. The minimum acidification time required for the 0.5%, 1.5%, and 2.5% alginate beads to completely gel in the acidified oil phase was determined to be 2 min as shown in Figure 7a by the absence of CaCO_3 particles (black spots) in the bead center.

The viability of MIN6 cells encapsulated using the microchannel emulsification process with the minimum required acidification time of 2 min was then compared to the viabilities of cells after 4 or 10 min of acidification. As shown in Figure 7b,c, there was a significant effect of the bead residence time in acid on the encapsulated MIN6 cell viability. A longer residence time allows more time for acetic acid to partition into the alginate phase, potentially decreasing the local pH near the cells as well as increasing cell exposure time to this low pH. The live/dead fluorescence microscopy images depicted in Figure 7b show that the acidification time of 2 min resulted in the highest viability of $89 \pm 2\%$, similar to the viability obtained using stirred emulsification ($\sim 90\%$),¹³ and the acidification time of 10 min resulted in the lowest viability ($67 \pm 11\%$). Similarly, cells recovered from degelled beads show a decrease in cell viability from $61 \pm 4\%$ to $27 \pm 6\%$ upon increasing the acidification time from 2 to 10 min (Figure 7c). Bead degelling and flow cytometry results may underestimate viability compared to in situ live/dead staining of the encapsulated cells due to cell death during the degelling process. When comparing viability losses at different stages

of the microchannel emulsification process, the main step leading to cell death was the acidification and internal gelation step rather than cell passage through the microchannels (Figure 7d). This suggests that improved pH control, potentially through buffer selection, could further improve cell survival, as shown in previous stirred emulsification viability studies.¹³

3.7 | Impact and future directions

Unlike previous microchannel emulsification processes, this novel device can form a water-in-oil emulsion whereby simultaneous emulsification and internal gelation processes result in monodisperse gelled alginate beads encapsulating cells. The device can overcome the challenges associated with conventional nozzle encapsulation devices, including reaching clinical-scale production rates of 140 mL/hr per microchannel, without substantially increasing process complexity. The device also produces droplets much more uniform in diameter than those produced using stirred emulsification. The microchannel emulsification process has the flexibility to reach a wide variety of applications aside from islet transplantation and Type 1 diabetes treatment. Bead production can be achieved over a wide range of alginate types, concentrations, molecular weights, viscosities, and gelling conditions. Hence, the stability and permeability of resulting beads could be tuned to fit the application, which may range from the controlled release of microorganisms in agriculture applications, to masking unpleasant tastes in certain foods, or to the immunoisolation of tissues or biologically-active substances.

Although the beads produced in this work were larger than the initial target, larger beads have shown increased mechanical stability in vivo with significantly reduced fibrosis.⁴⁸ However, a smaller bead diameter may reduce the acid concentration needed for complete bead gelation, improving the viability of encapsulated cells. Smaller beads can be achieved by modifying temperature, emulsifiers, and microchannel dimensions, although a lower channel dimension limit exists to prevent islet damage or channel obstruction. With pluripotent stem cell-derived islets, it may be possible to manufacture smaller islet-like clusters, which will reduce hypoxia as well as allow the use of smaller microchannels. The bead production rate can also be increased simply by milling more microchannels through the PTFE plates. Following the continued development of the microchannel emulsification

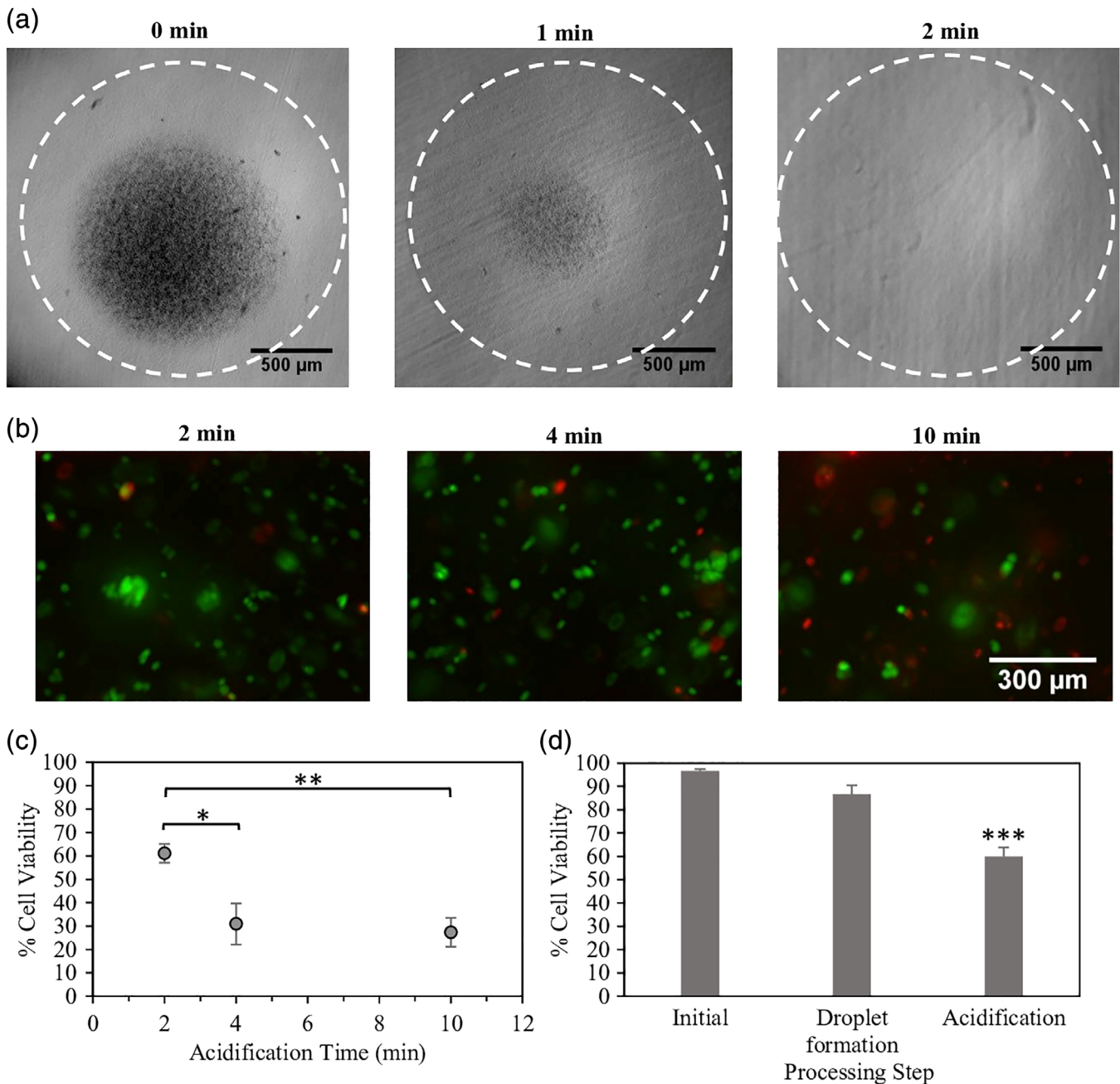


FIGURE 7 Effect of processing steps on beta cell survival. (a) Observed CaCO_3 particle dissolution at different acidification times. (b) MIN6 cell survival at different acidification times visualized by calcein AM (live/green) and ethidium homodimer (dead/red) staining. (c,d) MIN6 cell survival quantified by flow cytometry at various (c) acidification times and (d) microchannel emulsification processing steps (initial, droplet formation before acid exposure, and acidification/internal gelation). * $p < .05$; ** $p < .01$; *** $p < .001$

process to achieve scalable, adaptable, and robust generation of alginate beads, the widespread use of microchannel emulsification is envisioned.

4 | CONCLUSIONS

In this study, a novel microchannel emulsification device was developed to produce monodisperse alginate beads for beta cell encapsulation. Optimization of the device led to the generation of alginate beads at higher production rates than conventional nozzle encapsulation devices and higher uniformity than stirred emulsification. MIN6 cells

were successfully encapsulated using the microchannel emulsification process with encapsulated cell viabilities reaching ~89%. The current process was developed with the purpose of beta cell encapsulation for Type 1 diabetes cellular therapy; however, the process is widely applicable for immunoisolation of any cell type or 3D cell culture.

ACKNOWLEDGMENTS

We thank Galyna Shul (surface tension measurements), Ranjan Roy (contact angle measurements), Gad Sabbatier (computer-assisted design

drawing), and Zhiqing Liang (cell viability) for technical support, CMC Microsystems for access to the laser mill and microfabrication support, and Eva Habankova from the Polymer Institute SAS for evaluation of alginate molecular weights by SEC analysis. C.M.E.B. received a CGS M scholarship from the National Science and Engineering Research Council (NSERC) of Canada. Financial support was provided by an NSERC Discovery Grant (NSERC RGPIN 06271-15), the New University Researcher Start-up Program of the Fonds de Recherche du Québec—Nature et technologies, the Canadian Foundation for Innovation, the Canada Research Chair (NSERC Tier 2) (950-231290), and the Slovak Research and Development Agency under the contract number APVV-14-0858. C.M.E.B. and C.A.H. were funded by the Quebec Cell, Tissue and Gene Therapy Network –ThéCell (a thematic network supported by the Fonds de recherche du Québec—Santé). They are also members of the Centre Québécois sur les Matériaux Fonctionnels, PROTEO (the Quebec Network for Research on Protein Function) and the Montreal Diabetes Research Center (MDRC).

ORCID

Christina M.E. Bitar  <https://orcid.org/0000-0001-8707-6902>

Karen E. Markwick  <https://orcid.org/0000-0003-1891-8234>

Dušana Trelová  <https://orcid.org/0000-0002-9836-2469>

Zuzana Kroneková  <https://orcid.org/0000-0002-0265-8901>

Chloé M.O. Selerier  <https://orcid.org/0000-0002-8299-842X>

James Dietrich  <https://orcid.org/0000-0002-5205-7610>

Igor Lacik  <https://orcid.org/0000-0001-6037-3747>

Corinne A. Hoesli  <https://orcid.org/0000-0002-5629-7128>

REFERENCES

- Shapiro AM, Pokrywczynska M, Ricordi C. Clinical pancreatic islet transplantation. *Nat Rev Endocrinol*. 2017;13(5):268-277.
- Lim F, Sun AM. Microencapsulated islets as bioartificial endocrine pancreas. *Science*. 1980;210(4472):908-910.
- de Vos P, Marchetti P. Encapsulation of pancreatic islets for transplantation in diabetes: the untouchable islets. *Trends Mol Med*. 2002;8(8):363-366.
- Scharp DW, Marchetti P. Encapsulated islets for diabetes therapy: history, current progress, and critical issues requiring solution. *Adv Drug Deliv Rev*. 2014;67:35-73.
- Pellegrini S, Cantarelli E, Sordi V, Nano R, Piemonti L. The state of the art of islet transplantation and cell therapy in type 1 diabetes. *Acta Diabetol*. 2016;53(5):683-691.
- Desai T, Shea LD. Advances in islet encapsulation technologies. *Nat Rev Drug Discov*. 2017;16(5):338-350.
- Koch S, Schwinger C, Kressler J, Heinzen C, Rainov NG. Alginate encapsulation of genetically engineered mammalian cells: comparison of production devices, methods and microcapsule characteristics. *J Microencapsul*. 2003;20(3):303-316.
- Whelehan M, Marison I. Microencapsulation using vibrating technology. *Journal of Microencapsulation*. 2011;28:669-688.
- Poncellet D, Neufeld R, Bugarski B, Amsden BG, Zhu J, Goosen MFA. A parallel plate electrostatic droplet generator: parameters affecting microbead size. *Appl Microbiol Biotechnol*. 1994;42(2-3):251-255.
- Prusse U, Jahnz P, Wittlich J, Bredford J, Vorlop KD. *Bead Production with JetCutting and Rotating Disc/Nozzle Technologies*. Braunschweig, Germany: Bundesforschungsanstalt für Landwirtschaft; 2002:1-10.
- de Vos P, de Haan BJ, Kamps JA, Faas MM, Kitano T. Zeta-potentials of alginate-PLL capsules: a predictive measure for biocompatibility? *J Biomed Mater Res A*. 2007;80(4):813-819.
- Strand BL, Ryan L, Veld PI, et al. Poly-L-lysine induces fibrosis on alginate microcapsules via the induction of cytokines. *Cell Transplant*. 2001;10(3):263-275.
- Hoesli CA, Raghuram K, Kiang RLJ, et al. Pancreatic cell immobilization in alginate beads produced by emulsion and internal gelation. *Biotechnol Bioeng*. 2011;108(2):424-434.
- Hoesli CA, Kiang RL, Mocinecova D, et al. Reversal of diabetes by betaTC3 cells encapsulated in alginate beads generated by emulsion and internal gelation. *J Biomed Mater Res B Appl Biomater*. 2012;100(4):1017-1028.
- Poncellet D, Lencki R, Beaulieu C, Halle JP, Neufeld RJ, Fournier A. Production of alginate beads by emulsification/internal gelation. I. Methodology. *Appl Microbiol Biotechnol*. 1992;38(1):39-45.
- De Vos P, De Haan B, Wolters GH, Van Schilfgaarde R. Factors influencing the adequacy of microencapsulation of rat pancreatic islets. *Transplantation*. 1996;62(7):888-893.
- Avgoustiniatos ES, Colton CK. Effect of external oxygen mass transfer resistances on viability of immunoisolated tissue. *Ann N Y Acad Sci*. 1997;831:145-167.
- Bochenek MA, Veiseh O, Vegas AJ, et al. Alginate encapsulation as long-term immune protection of allogeneic pancreatic islet cells transplanted into the omental bursa of macaques. *Nat Biomed Eng*. 2018;2(11):810-821.
- Kobayashi I, Uemura K, Nakajima M. Formulation of monodisperse emulsions using submicron-channel arrays. *Colloid Surf A*. 2007;296(1-3):285-289.
- Kobayashi I, Wada Y, Uemura K, Nakajima M. Generation of uniform drops via through-hole arrays micromachined in stainless-steel plates. *Microfluid Nanofluid*. 2008;5(5):677-687.
- Sugiura S, Nakajima M, Iwamoto S, Seki M. Interfacial tension driven monodispersed droplet formation from microfabricated channel array. *Langmuir*. 2001;17(18):5562-5566.
- Charcosset C, Fessi H. Membrane emulsification and microchannel emulsification processes. *Reviews in Chemical Engineering*. 2005;21:1-32.
- Sugiura S, Oda T, Izumida Y, et al. Size control of calcium alginate beads containing living cells using micro-nozzle array. *Biomaterials*. 2005;26(16):3327-3331.
- Papajová E, Bujdoš M, Chorvát D, Stach M, Lacik I. Method for preparation of planar alginate hydrogels by external gelling using an aerosol of gelling solution. *Carbohydr Polym*. 2012;90(1):472-482.
- Maa JY, Lin YB, Chen XL, Zhao BT, Zhang J. Flow behavior, thixotropy and dynamical viscoelasticity of sodium alginate aqueous solutions. *Food Hydrocolloid*. 2014;38:119-128.
- Storz H, Zimmermann U, Zimmermann H, Kulicke WM. Viscoelastic properties of ultra-high viscosity alginates. *Rheologica Acta*. 2010;49(2):155-167.
- Rudawska A, Jacniacka E. Analysis for determining surface free energy uncertainty by the Owen-Wendt method. *Int J Adhes Adhes*. 2009;29(4):451-457.
- Carpenter AE, Jones TR, Lamprecht MR, et al. CellProfiler: image analysis software for identifying and quantifying cell phenotypes. *Genome Biol*. 2006;7(10):R100.
- Hoesli CA, Kiang RLJ, Raghuram K, et al. Mammalian cell encapsulation in alginate beads using a simple stirred vessel. *J Vis Exp*. 2017;(124):e55280. <https://doi.org/10.3791/55280>.
- Qi MRG, Morch Y, Lacik I, et al. Survival of human islets in microbeads containing high guluronic acid alginate crosslinked with Ca²⁺ and Ba²⁺. *Xenotransplantation*. 2012;19(6):355-364.
- Kroneková Z, Pelach M, Mazancová P, et al. Structural changes in alginate-based microspheres exposed to in vivo environment as revealed by confocal Raman microscopy. *Sci Rep*. 2018;8(1):1637.
- Miyazaki J-I, Araki K, Yamato E, et al. Establishment of a pancreatic β cell line that retains glucose-inducible insulin secretion: special

- reference to expression of glucose transporter isoforms. *Endocrinology*. 1990;127(1):126-132.
33. Kobayashi I, Nakajima M, Mukataka S. Preparation characteristics of oil-in-water emulsions using differently charged surfactants in straight-through microchannel emulsification. *Colloids Surf A Physicochem Eng Asp*. 2003;229(1):33-41.
 34. Surface Tension, Solid Surface Energy Data (SFE) for Common Polymers. <http://www.surface-tension.de/solid-surface-energy.htm>. Accessed January 14, 2017.
 35. Sahlin E, Beisler AT, Woltman SJ, Weber SG. Fabrication of microchannel structures in fluorinated ethylene propylene. *Anal Chem*. 2002;74(17):4566-4569.
 36. Owens DK, Wendt RC. Estimation of surface free energy of polymers. *J Appl Polym Sci*. 1969;13(8):1741-1747.
 37. Sugiura S, Nakajima M, Seki M. Effect of channel structure on microchannel emulsification. *Langmuir*. 2002;18(15):5708-5712.
 38. Kobayashi I, Mukataka S, Nakajima M. Effect of slot aspect ratio on droplet formation from silicon straight-through microchannels. *J Colloid Interf Sci*. 2004;279(1):277-280.
 39. Fernandez S. Emulsion-based islet encapsulation: predicting and overcoming islet hypoxia. *Bioencapsul Innov*. 2014;220:14-15.
 40. Gu H, Duits MHG, Mugele F. Droplets formation and merging in two-phase flow microfluidics. *Int J Mol Sci*. 2011;12(4):2572-2597.
 41. Sugiura S, Nakajima M, Kumazawa N, Iwamoto S, Seki M. Characterization of spontaneous transformation-based droplet formation during microchannel emulsification. *J Phys Chem B*. 2002;106(36):9405-9409.
 42. Lucio AA, Mongera A, Shelton E, Chen R, Doyle AM, Campàs O. Spatiotemporal variation of endogenous cell-generated stresses within 3D multicellular spheroids. *Sci Rep*. 2017;7(1):12022.
 43. Xu JH, Li SW, Tan J, Luo GS. Correlations of droplet formation in T-junction microfluidic devices: from squeezing to dripping. *Microfluid Nanofluid*. 2008;5(6):711-717.
 44. Vladislavljevic GT, Kobayashi I, Nakajima M. Effect of dispersed phase viscosity on maximum droplet generation frequency in microchannel emulsification using asymmetric straight-through channels. *Microfluid Nanofluid*. 2011;10(6):1199-1209.
 45. Rokstad AMA, Lacik I, de Vos P, Strand BL. Advances in biocompatibility and physico-chemical characterization of microspheres for cell encapsulation. *Adv Drug Deliv Rev*. 2014;67:111-130.
 46. Mørch YA, Donati I, Strand BL. Effect of Ca^{2+} , Ba^{2+} , and Sr^{2+} on alginate microbeads. *Biomacromolecules*. 2006;7(5):1471-1480.
 47. Thanos C, Calafiore R, Basta G, et al. Formulating the alginate-polyornithine biocapsule for prolonged stability: evaluation of composition and manufacturing technique. *J Biomed Mater Res A*. 2007;83(1):216-224.
 48. Veisoh O, Doloff JC, Ma M, et al. Size- and shape-dependent foreign body immune response to materials implanted in rodents and non-human primates. *Nat Mater*. 2015;14(6):643-651.

How to cite this article: Bitar CME, Markwick KE, Trelóvá D, et al. Development of a microchannel emulsification process for pancreatic beta cell encapsulation. *Biotechnol Progress*. 2019;35:e2851. <https://doi.org/10.1002/btpr.2851>